Proceedings of the ASME 2012 International Design Engineering Technical Conferences &
Computers and Information in Engineering Conference
IDETC/CIE 2012
August 12-15, 2012, Chicago, IL, USA

DETC2012-70122

A MICRO-SCALE MAGNETIC TUMBLING MICROROBOT

Wuming Jing
Multi-Scale Robotics Lab
Mechanical Engineering Department
Stevens Institute of Technology
Hoboken, New Jersey 07030
Email: wjing@stevens.edu

Nicholas Pagano
Multi-Scale Robotics & Automation Lab
Mechanical Engineering Department
Stevens Institute of Technology
Hoboken, New Jersey 07030
Email: npagano@stevens.edu

David J. Cappelleri[*]
Assistant Professor
Mechanical Engineering Department
Stevens Institute of Technology
Hoboken, New Jersey 07030
Email: david.cappelleri@stevens.edu

ABSTRACT

This paper presents a magnetic tumbling microrobot design at the micro-scale. The microrobot has a dumbbell shape whose largest dimension is about 400 μm. When subjected to an exterior predefined magnetic field, the magnetic microagent performs a tumbling motion driven by the interacting magnetic forces and momentums. The magnetic field providing driven force is generated by a coil system consisting of five electromagnetic coils. Under the available driven field, we show that the prototype agent is able to tumble on various types of surfaces in both dry and fluid environments.

1 Introduction

Untethered submillimeter mircrorobotics has emerged within the last decade with the attractive features due to the small size and working mode. As one of the next waves in intelligent systems, microrobots have shown potential on advanced manufacturing, the health care industry and the continued miniaturization of consumer products [1], especially in biotechnology and medical applications [2], such as minimally invasive surgery and targeted drug delivery. These needs highlight the advantages of certain microrobotic features: untethered operation and small size, which also indicates design and manufacturing challenges at the the same time. Aside from the wireless requirement, there is no cell or any energy storage device available in this scale.

More than the power, locomotion mechanisms still need delicate designs to achieve controllable motion.

To realize veritable submillimeter untethered mobile microrobot, a few agents with different working principles have been designed and developed in the near past. The first representative work was done by Donald et al. [3–5] applying electrostatic principles. The MEMS fabricated device consisted of a cantilevered steering arm mounted on an scratch drive actuator (SDA), where both were made of conductive polysilicon. The microrobot was driven and steered by an engineered surface with buried electrical grids. Sul [6] et al. developed a thermally actuated locomotive device which consisted of three-legged, thin-metal-film bimorphs. The device was able to perform stepwise translation on a low friction surface through curvatures of legs induced by a focus laser. Different laser energy and parameters controlled the velocity and motion direction of the agent. Although these two types of microrobots have shown fancy motion and control, their operating principles limit their application potential especially in the bio and medical fields. This is because it is difficult to incorporate an engineered surface into a living body for surgical application and also risky to apply the high voltage needed to power the device. The thermal actuation mechanism method faces a similar problem, which lies in the laser power delivery for a minimally invasive surgery site or in a cluttered biological environment.

Compared to the electrostatic and thermal principled devices, magnetic fields can provide attractive features for power and control. Frutiger et al. [7, 8] developed one delicate micro

---

[*]Address all correspondence related to the research in this publication to Professor David J. Cappelleri.
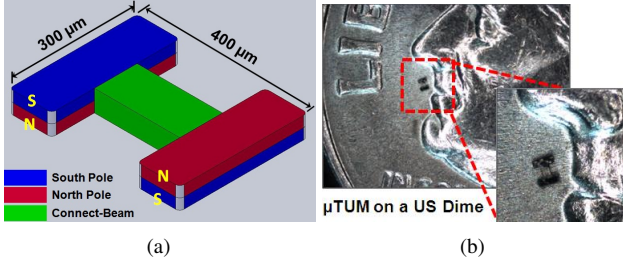
FIGURE 1. The μTUM magnetic tumbling microrobot. (a) Schematic of μTUM. (b) μTUM on a US dime.

agent named the MagMite. The device is made of two nickel soft magnetic bodies connected by a gold nonmagnetic spring, so it can harvest energy for the external oscillating gradient magnetic field and transform it into into inertia- and impact-driven mechanical forces while being fully controllable. Another design applying magnetic energy was developed by Pawashe et al. [9, 10] using NdFeB permanent magnetic material. This microrobot made of a hard magnetic piece can perform stick-slip motion under alternating gradient magnetic fields. Both of the magnetic micro devices are able to do omnidirectional translation on surfaces in dry or fluidic environments. The limitation of these two designs is that the motion mechanism requires a relatively idealized environment. Therefore it is difficult to realize the oscillating or stick-slip motion in non-ideal environments even if the magnetic field intensity is greatly increased.

Real bio-environments are usually not flat but complex surfaces of flagella or tissue. Schoen et al. [11, 12] investigated micropatterned treads with different designs for in vivo robotic mobility and they also characterized the mechanical properties of the small bowel. The result showed the anisotropical behaviors of the tissue and the mucoadhesion. So we need more adaptable mechanisms for complex surface conditions in bio medical applications. Recently, Tou et al. [13, 14] designed a rolling locomotion method for magnetic microrobots. An external rotating magnetic field was generated by a rotating permanent magnetic block underneath the working surface. The magnetic force along with normal blocking and friction force enables successive rotations. Besides translation on a plane, this microrobot can also climb slopes. One limitation of this design is that workspace is confined within the certain travel distance of the permanent magnetic body underneath. If the robot rolls too far from the driven piece, it will be pulled back instead of rolling farther.

In this work we present a novel untethered tumbling magnetic robot (μTUM) with a dumbbell type structure (Fig. 1) which can perform tumbling locomotion with predefined magnetic field signals. First, we introduce the design of the micro agent and its working mechanism. Then, we introduce the coil drive system followed by validating the mechanism through magnetic field and force analysis. After the fabrication process
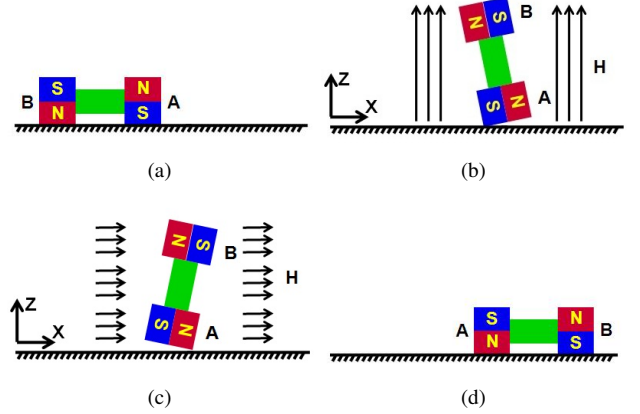

FIGURE 2. Motion mechanism of the magnetic tumbling microrobot. (a) Initial position; (b) Apply vertical magnetic field to erect the agent; (c) Apply horizontal magnetic field to finish the tumbling; (d) Final position of one tumble action.

for the μTUM agents is introduced, the experimental results are presented. Finally, we conclude with a discussion and suggestions on improving work performance.

2 Tumbling Magnetic Microrobotic Design and Motion Mechanism

2.1 Microrobot Design

A tumbling robot at the small scales can be more adaptable for complex surface conditions, such as convex shapes and slopes, than traditional microrobot designs. The advantage of tumbling locomotion at the micro scale is that it needs less driving force compared to the direct pulling motion by gradient magnetic fields. The tumbling mechanism mainly just needs to conquer gravity (inertial forces) to accomplish its motion cycle. The direct pulling method needs to conquer friction resistance which is much larger than the gravity force on the micro scale. This is key because the large driving forces required can be a big problem for the magnetic locomotion principle at small scales. Both distance and agent volume scaling down will dramatically decrease the magnetic force required for actuation. However, the surface forces (static friction) to induce locomotion can be quite large and result in uncontrollable locomotion. As a relatively unexplored locomotion mechanism, tumbling shows potential to provide increased mobility on smaller scales [15] with smaller actuation force. To realize the tumbling motion in submillimeter dimensions, a composite magnetic structure of a dumbbell shape has been designed (Fig. 1). The two bell parts of the dumbbell structure are permanent magnets with opposite polar directions. The bells are connected by a non magnetic bridge piece.

2.2 Motion Mechanism

Suppose the agent lies on the working surface (Fig. 2(a)). When the magnetic field of upward direction ($+z$) turns on (Fig. 2(b)), bell A will be pulled down while bell B will be repelled up. This pair of forces will generate a momentum. This momentum plus gravity, along with the resultant blocking force will cause the device to stand up in an equilibrium stance (transient state). If we turn off this vertical magnetic field at the transient state, this device would fall back to surface to its original position. But if we turn on another horizontal magnetic field pointing right ($+x$) at the same time with turning off the vertical field (Fig. 2(c)), the dumbbell device will experience a continuous momentum making itself tumble forward. Thus, the device will fulfill a tumbling cycle naturally with turning off the the horizontal magnetic field (Fig. 2(d)). If the device needs to tumble to the left, all we need to do is to turn on the magnetic field in the opposite direction. To easily adjust the device's orientation in the horizontal plane, we can keep the device in the transient state by holding the vertical magnetic field on and then steer the agent's heading by steering the horizontal magnetic field direction. Only low field intensity is needed here because of the low friction due to the small contact area. The beauty of this tumbling mechanism is the adaptability to different non-idealized surfaces mentioned above. During this locomotion process the surface does not need to be perfectly flat or horizontal as long as it has contact between the microrobot and the surface.

3 Magnetic Coil Drive System

To fulfill the motion of tumbling mechanism with the sub-millimeter magnetic microrobot, a test bed consisting of five independently controlled coils has been constructed with electromagnetic wire of the same gauge (Fig.3). One coil is built with more turns than the others and mounted as the bottom coil to provide the vertical magnetic field. The other four coils are manufactured identically with the same dimensions and number of turns to produce the horizontal magnetic fields. All five coils have cobalt-iron core inserts with high magnetic permeability which dramatically increases the field strength. The coil facts are summarized in Table 1. The work space area encompassed by the coil set is one square inch. The realtime imaging is accomplished by an overhead CCD camera (Point Grey FL2-14S3C, *www.ptgrey.com*) along with a microscope lens (Edmund VZM 300i, *www.edmundoptics.com*) of adjustable magnification. The combination is able to provide a $8.0mm \times 2.0mm$ field of view. A side camera with similar optics also exists in the test-bed. The coils are controlled by individual series of solid state relays. Customized signals are sent via computer control of a data acquisition board (LabJack U3-HV and CB15, *www.labjack.com*). The system can pulse signals with frequencies as high as 100 kHz.
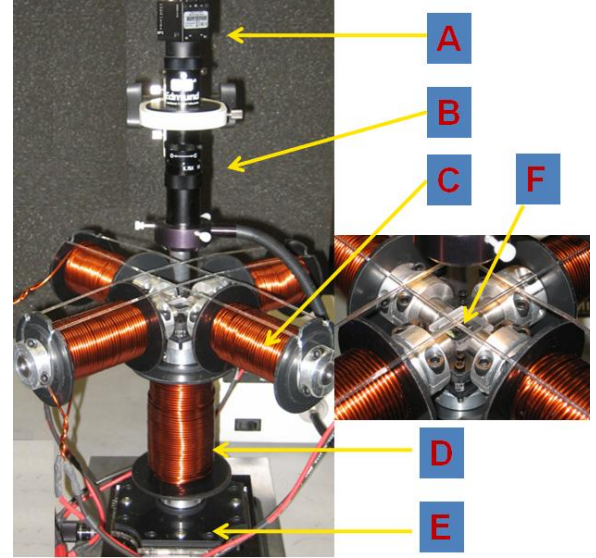

FIGURE 3. Photograph of the electromagnetic test bed. (A) CCD camera; (B) Microscope lens; (C) One of the four side coils set for the horizontal magnetic field; (D) Bottom coil for the vertical magnetic field; (E) X-Y stage; (F) Chamber in workspace. Side camera and optics are not pictured.

TABLE 1. Parameters of Electromagnetic coils

Facts	Vertical coil	Horizontal coils
Number of Turns	700	320
Inner Diameter (mm)	17.3	17.3
Outer Diameter (mm)	60	48
Length (mm)	110	90
Core Material	CoFe	CoFe
Relative Permeability	70	70

4 Theoretical Analysis

The overall system design has to be calculated and analyzed before the fabrication and testing of this novel μTUM microrobot. Based on the intensity of the magnetic field and the agent's magnetization, we can know whether the agent will stand up in transient state to fulfill the tumbling. The following force analysis is necessary to predict the motion.

4.1 Magnetic Field

The magnetic field intensity is determined by the input current (I) while the magnetic induction is due to the permeabil-

ity of the material. So we choose to have electromagnetic coils wrapped on a core with a high permeability value to provide the magnetic field. The magnetic field due to a current-carrying closed loop can be calculated based on the Bio-Savart law [16]:

$$\boldsymbol{B} = \frac{\mu_0}{4\pi} \oint_C \frac{I d\boldsymbol{l} \times \hat{\boldsymbol{r}}}{r^2} \quad (1)$$

where $\boldsymbol{B}$ is the magnetic field at the desired space point, μ_0 is the permeability of air ($4\pi \times 10^{-7} H \cdot m^{-1}$), I is the current flowing in the closed loop, $d\boldsymbol{l}$ is the differential element of the current-carrying wire, and $\boldsymbol{r}$ is the displacement vector pointing from the wire element to space point computed, where $\hat{\boldsymbol{r}}$ is the unit vector is this direction and r indicates the magnitude of this vector. Since the magnetic field at an arbitrary space point obeys the principle of superposition, the total magnetic field intensity generated by a solenoid can be determined as:

$$\boldsymbol{B} = \int_{L_1}^{L_2} \frac{\mu_0}{4\pi} \oint_C \frac{I d\boldsymbol{l} \times \hat{\boldsymbol{r}}}{r^2} \quad (2)$$

where L_1 indicates the loop on one end of the solenoid and L_2 indicates the one on the other end, while the other symbols hold the same notions with Eq. 1. If a core of high permeability μ is inserted inside the solenoid, the magnetic field $\boldsymbol{B}$ can be increased by μ times accordingly. Further, the magnetic field intensity caused by multiple solenoids can be derived through the algebraic sum of each one's contribution.

Assume the wire turns are distributed uniformly in space, theoretical calculations with Eq. 2 and Table 1 show that both the vertical and horizontal coils are able to provide magnetic fields of about 5 mT at a half inch distance (center of the workspace) when 1A of current is flowing in the wire loop, with the gradient of the field around 500 $mT \cdot m^{-1}$. This theoretical estimation is corroborated by a DC Gaussmeter (AlphaLab Inc. *http://www.trifield.com/*) which works with the Hall effect principle. The magnetic field generated by the coil system has been modeled and simulated in a 1:1 ratio using COMSOL software (*www.comsol.com*) (Fig.4). The results are consistent with the measurements and theoretical calculations.

4.2 Force Analysis

Any magnetized body within a magnetic field will experience force and torque, which is the basic principle for the design of magnetic microrobotics [17–21]. The magnetized body always has the tendency to align its internal magnetization into the alignment with the external field. In any case, the acting force on the magnetic body is in the gradient direction of the magnitude of the applied field. The general case of this acting force density
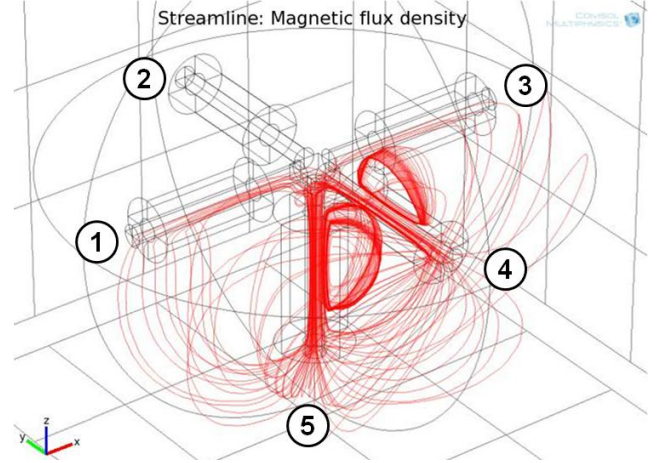

FIGURE 4. Simulation of magnetic field generated by the electromagnetic coil system. Coil 4 and 5 are activated.

is [22]:

$$\boldsymbol{F}_{md} = -\mu_0 \bigtriangledown \left[\int_0^H \left(\frac{\partial Mv}{\partial v} \right)_{H,T} dH \right] + \mu_0 (\boldsymbol{M} \cdot \bigtriangledown) \boldsymbol{H} \quad (3)$$

where $\boldsymbol{F}_{md}$ is the magnetic force density, $\boldsymbol{H}$ is the internal field of the magnetized body (not the external field applied), T is the temperature, $\boldsymbol{M}$ is the magnetization, v is the volume. Hence $Mv = \boldsymbol{\sigma}$, which is the magnetic moment per kg of the magnet.

In this work, the neodymium magnet (NdFeB) is applied in the magnetic part of the microrobot. The advantage of this permanent magnetic material is the high remanence and extremely high coercivity. Thus, to simplify the calculations, we treat the magnitude of the inner field strength H as constant value, which is 600 ($kA \cdot m^{-1}$). So the acting force and torque can be derived through:

$$\boldsymbol{F}_m = V_m (\boldsymbol{M} \cdot \bigtriangledown) \boldsymbol{B} \quad (4)$$

$$\boldsymbol{\tau}_m = V_m \boldsymbol{M} \times \boldsymbol{B} \quad (5)$$

where $\boldsymbol{F}_m$ and $\boldsymbol{\tau}_m$ are the acting force and torque on the magnetic body respectively, and V_m is the volume of magnetic part. So with the facts of the μTUM microrobot (Table 2), we can determine that one bell part will get about 30 nN acting force (This force is calculated in the example scenario referred in the above section), while the total gravity force of the μTUM is around 0.06 nN.

After deriving the magnetic force, the general case of force analysis for the tumbling robot is examined. As shown in Fig.5,

TABLE 2. Parameters of μTUM Microrobot

Facts	Bell Part	Bridge Part
Length(μm)	100	200
Width(μm)	300	100
Thickness(μm)	50	50
Material	SU8, NdFeB	SU8
Magnetic volume(μm^3)	9.4×10^4	0
Density($kg \cdot m^{-3}$)	1,600	1,200
Gravity(nN)	0.024	0.012

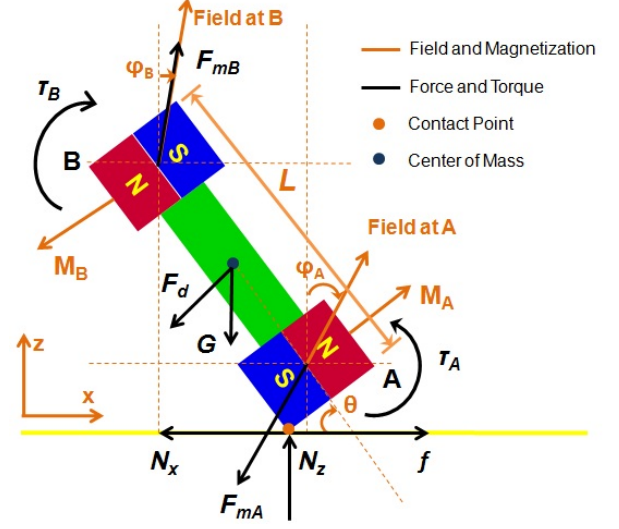Note: The magnetic volume is derived by the mass/volume ratio used to mix the NdFeB powder in SU8 photoresist.

FIGURE 5. Free body diagram of μTUM microrobot on a surface with applied external forces and torques.

the arrows in orange color indicate the directions of the magnetic field or the magnetization of the bell parts. The ones in black show the forces and torques that could act on the agent. φ_A and φ_B are the angle contained by the vertical direction of the streamline of magnetic field at position A or B, respectively, whereas θ is the agent's inclined angle from the horizontal surface. Then general forces on the microrobot in x-z plane can be expressed as:

$$
\begin{cases}
m\ddot{z} = \Sigma F_z = F_{mBz} - G - F_{mAz} - F_a - F_{dz} + N_z, \\
m\ddot{x} = \Sigma F_x = F_{mBx} + f - F_{mAx} - F_{dx} - N_x, \\
I_m \ddot{\theta} = \Sigma \tau \\
\qquad = \tau_B - \tau_A + (F_{mBz} + F_{mAz} - N_z + F_{ad})\dfrac{L}{2}cos\theta \\
\qquad - (f - N_x + F_{mBx} + F_{mAx})\dfrac{L}{2}sin\theta
\end{cases}
\tag{6}
$$

where m is the mass of the micro agent, I_m is the moment of inertia about the center of mass, L is the length of the agent, F_m and τ are the magnetic force and torque acting on the bell parts respectively, G is the gravity force, F_a is the surface adhesion, F_d is the damping force if the agent works in fluid environment, N is the blocking force and f is the resulting friction force where $f = \mu N_z$, μ is the Coulomb friction coefficient. Subscript x and z show the direction. Note that subscript A and B indicate the two bell parts, while normal B means the magnetic flux intensity elsewhere. Based on Eq.4 and 5, the magnitude of the magnetic

force and torque can be calculated with:

$$
\begin{cases}
F_{mAx} = V_A M_A \triangledown B_A sin\phi_A cos(\frac{\pi}{2} - \theta) \\
F_{mAz} = V_A M_A \triangledown B_A cos\phi_A cos\theta \\
F_{mBx} = -V_B M_B \triangledown B_B sin\phi_B cos(\frac{\pi}{2} + \theta) \\
F_{mBz} = V_B M_B \triangledown B_B cos\phi_B cos(\pi - \theta) \\
\tau_A = V_A M_A B_A sin(\theta - \varphi_A) \\
\tau_B = V_B M_B B_B sin(\pi - \theta + \varphi_B)
\end{cases}
\tag{7}
$$

where B is the magnetic flux intensity, $\triangledown B$ is the gradient of the flux intensity, V and M are the volume and magnetization of the bell parts. From Eq.6 and Eq.7 we can recognize the influence of surface and magnetic field on the agent's behaviors, which is able to be summarized into the following categories:

1) Slipping case: $\Sigma F_x = 0$, $\Sigma F_z \leq 0$, $\Sigma \tau > 0$. The surface is at perfect horizontal plane ($N_x=0$) without friction ($f = 0$), adhesion ($F_a = 0$), or damping ($F_d = 0$), and the magnetic field is in the perfect vertical direction ($\varphi = 0$). In this extreme ideal case, although the agent will rotate in the $x - z$ plane, but without friction, only pure pure rotation is achieved which is not desired.

2) Pulling up case: $\Sigma F_z > 0$. If the summed forces in z direction are positive, no matter the results of ΣF_x and $\Sigma \tau$, the agent will be pulled up and fly out of the working plane. This is not an equilibrium state which is also not desired.

3) Sliding case: $\Sigma F_x \neq 0$, $\Sigma F_z \leq 0$. In this case, the agent will translate along the surface whereas the friction force f will be-

come sliding friction and turn to the opposite way to the direction shown in Fig.5. This sliding behavior will cause adverse effects on the tumbling motion which makes the motion control more difficult.

4) Tumbling case: $\Sigma F_x = 0, \Sigma F_z \leq 0, \Sigma \tau > 0$. The difference between this scenario and the sliding case is that there is friction in the x direction. This case indicates there is no sliding or pulling up, which means agent stays on the surface and the friction is static. The μTUM will perform pure tumbling motion in this case which is the desired control state.

5 μ**TUM Agent Fabrication**

This μTUM microrobot design has been fabricated through a custom surface micromachining process (Fig.6). At first, a 4" bare silicon wafer is prepared in step (1) and coated with OMNICOAT (MicroChem, *www.microchem.com*). This sacrificial layer assists the final release of the device. In following step (2), a pure photoresist SU8-50 (MicroChem, *www.microchem.com*) is coated and baked. This layer is patterned as the bridge part in step (3), which is used to connect the two bell parts of agent. To manufacture the magnetic bell part with specific polarization, magnetic particles are mixed with controlled mass density in the SU8-50. The magnetic particles are the grounded products of the NdFeB permanent magnetic powder (MQP A, Neo Material Technologies, *www.magnequench.com*), whose average size is smaller than the SU8-50 spinned thickness (about 50 μm). A customized mass/volume ratio is controlled during the mixing to know the volume of magnetic particles in a certain enclosed dimension. In order to configure the particles' polarization, we take advantage of the forming mechanism of SU8. In the soft bake process which evaporates the solvent in photoresist for solidification, a 4" diameter NdFeB disk (K&J Magnetics, *www.kjmagnetics.com*) is set underneath the silicon substrate while baking (step (4)). The polarization of the magnetic disk is along the thickness direction, so the bell part of the eventual micro agent will be magnetized in the thickness direction. Because the baking temperature of SU8-50 (95°C) is much lower than the Curie temperature of NdFeB material (above 300°C), the NdFeB disk will keep its magnetic property during the heating process. Also because of the excellent heat conductivity of metal, the disk between the sample and hotplate does not impact the baking result. After the soft bake, the magnetic photoresist layer is aligned and patterned as one bell part in step (5). Step (6) and (7) are the repeat of step (4) and (5) for the other magnetic bell part, whereas the polarization process during soft bake is the opposite. The baking process during photolithography will evaporate the solvent in photoresist. This fixes the NdFeB powder inside the photoresist. Therefore the polarization in step (6) will not reverse the polarization in step (4). Finally, a dumbbell structure with two magnetic bell parts of opposite polarization is achieved after the final release by PG remover (step (8)).
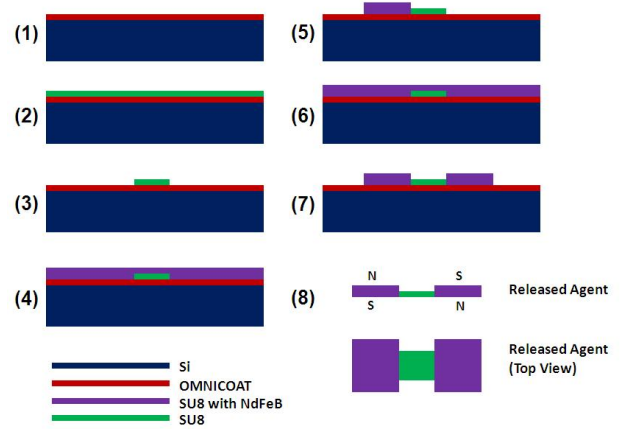

FIGURE 6. Schematic of fabrication process for the μTUM microrobot design.

6 **Experimental Results**

This proposed magnetic tumbling microrobot has been tested in the built electromagnetic coil system. Preliminary manually controlled tests have verified the design and fabrication method of the agents and the tumbling motion mechanism at the submillimeter scale. The orientation of the agent in horizontal plane has also been successfully steered.

6.1 **Polarization Test**

The two opposite polarized magnetic bell structures are the key to the tumbling motion mechanism. Therefore, the polarization result of the agent is tested before performing the motion tests. After releasing the agent, no feature can be recognized as polarization direction on the two bell structures. But we can tell the field direction of the electromagnetic coil by the right-hand rule. As shown in Fig.2(b), if the field line points upward, the bell part with N-end facing down will be lifted up. Therefore, with a known direction of magnetic field, the polarization of the bell part is able to be detected. Furthermore, to verify whether the polarization of the two bell parts are opposite, the current flowing in the bottom coil can be switched. Then, the direction of the vertical magnetic field will point downward, which means the bell part with S-end facing down will be repelled up. Results of such tests show that most of the μTUM are fabricated as desired (Fig.7). This proof of concept test also validates the fabrication method referred to previously for magnetic parts at the micro scale with desired polarization.

6.2 **Tumbling Motion Tests**

To test the feasibility of tumbling motion mechanism for the submillimeter agent, a proof of concept experiment is conducted step-by-step according to the proposed activation mechanism with manually controlled input signals to the coil system.
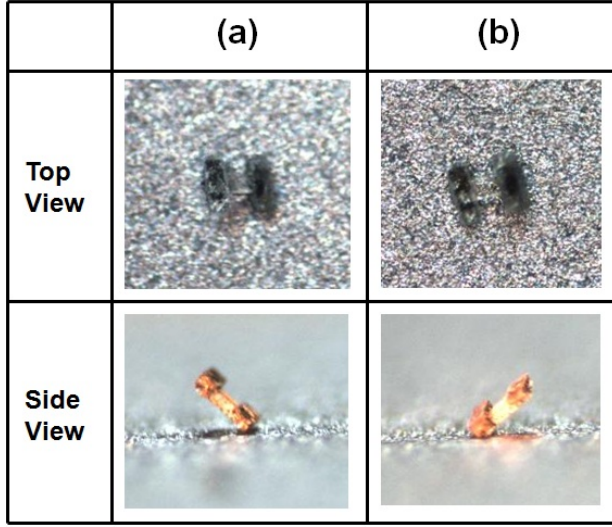
6

FIGURE 7. Polarization test of a μTUM agent. (a) and (b) are the response to the vertical field with opposite directions.

FIGURE 8. Steps in one cycle of a μTUM agent performing tumbling motion.

FIGURE 9. Steering tests after the μTUM agent reaches transient state.

These manually controlled tests verify that the μTUM agent is able to perform the tumbling motion (Fig.8) for locomotion.

According to the proposed tumbling motion mechanism (Fig.2), after the agent is set on the surface in the working space (Fig.8(a)),only the bottom coil is turned on. The direction this vertical magnetic field line is customized upwards by the current flow in the bottom coil, which corresponds to a magnet body with N-end on top. When the agent stands up in the transient state (Fig.8(b)), the facing orientation is judged by human observer, then the side coil located in the desired tumbling direction is turned on. The direction of this horizontal magnetic field line is customized to point away from the agent to the coil, which equals to a magnet body with S-end facing to the agent. The key of this control is to turn off the vertical field at the same time as turning on the horizontal field. Erratic response is observed in trial tests when this fails. The function of the horizontal field is to pull the agent past of upright position (Fig.8(c)). Only a short period of time is necessary for the corresponding side coil to be on. Thus, unlike the input signal of bottom coil, a pulse signal is used as an input for producing the fast horizontal field signal. A successful case is observed if the agent passes by the upright position and then falls down forward fulfilling a wholesome tumbling cycle (Fig.8(d)). Due to delays of the mechanical relay, this step can fail if the agent does not swing across the upright position. In this case the agent will fall back to its initial state.

6.3 Steering Tests

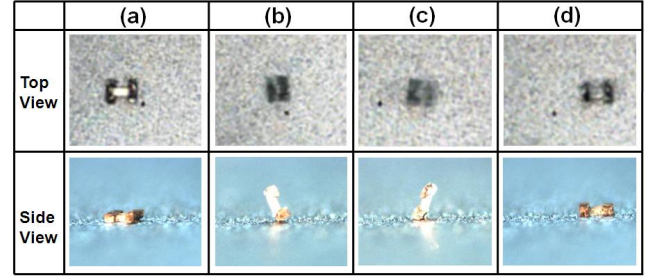Steering tests have also been conducted along with the tumbling motion tests. Without steering the orientation of the agent in horizontal plane, the tumbling motion can only be realized in the initial facing direction. So after achieving a steady transient state, horizontal magnetic fields from different planar directions are applied separately. The agent turns to face along the field line accordingly, as shown in Fig.9.
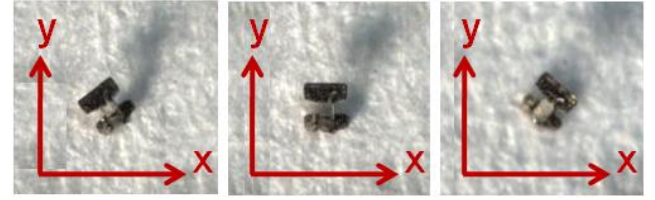
The key of successful steering is observed to be the flux intensity of the horizontal magnetic field. If the intensity of the horizontal field is comparable or even larger the the vertical one, the agent will be more likely to experience pulling than steering. So the important tip for steering is to turn on the horizontal magnetic field in the magnitude a certain amount lower than the vertical field.

6.4 Mobility Tests

Tests in the above section have shown the mobility of this μTUM magnetic microrobot design. The translation velocity v is able to be calculated out as:

$$v = \frac{L}{T} \qquad (8)$$

where L is the length of agent, T is the period time of the control signal to fulfill a tumbling cycle. For example, the L of the μTUM agent is 400 μm, the time of manually controlled signal to fulfill a cycle T is 1.03 s according to the recorded video. Thus the translation speed of $v = 0.38$ mm/s (≈ 1 $body\ length/s$) is expected when repeating the tumbling cycle. It is obvious that a faster control signal cycle will correspond to faster resulting
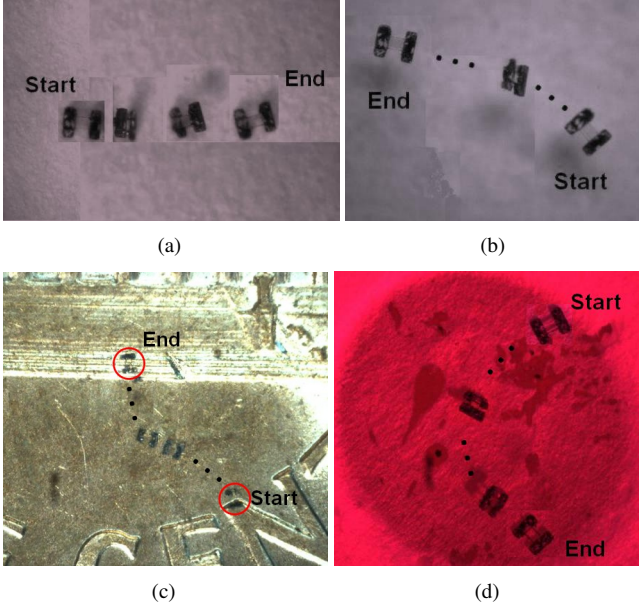
FIGURE 10. Tumbling motion test on various types of surfaces in dry and fluid environment. (a) On normal printing paper; (b) On a glass microscope slide; (c) On one side of a US penny in silicon oil; (d) On one cut of bio tissue in normal saline.

speeds.

Most of the mobility tests were conducted on the back side of a silicon wafer, which is rough, but flat. Based on the proposed tumbling motion mechanism, μTUM will be able to adapt to various types of surfaces and more complex environments. This feature is critical for future real bio-related applications. Therefore, mobility tests have also been conducted on other types of surfaces in both dry and fluid environments: normal printing paper (Fig.10(a)), a glass microscope slide (Fig.10(b)), on the surface of one US penny in silicon oil (Fig.10(c)), and on a biological tissue sample in normal saline (Fig.10(d)).

The paper and glass slide are meant to provide cross references for different surface frictions. It is noticed that a minimum inclined angle is necessary to fulfill the tumbling motion on certain surface, and also the more static friction the surface has, the less minimum inclined angle θ needed. It is noted sometimes there is a small initial inclined angle θ when the agent is set on these non-conductive surfaces with no current input. This initial inclined angle can be explained by surface charge and electrostatic forces. This phenomenon could also provide a feasible way to quantify the electrostatic force at the micro scale (nN scale force).

The tests on biological tissue sample and US penny are designed to test the mobility of the μTUM agent on non-flat surfaces of 3D structures, which are more similar to real bio-environments than flat surfaces. The trial tests show that the
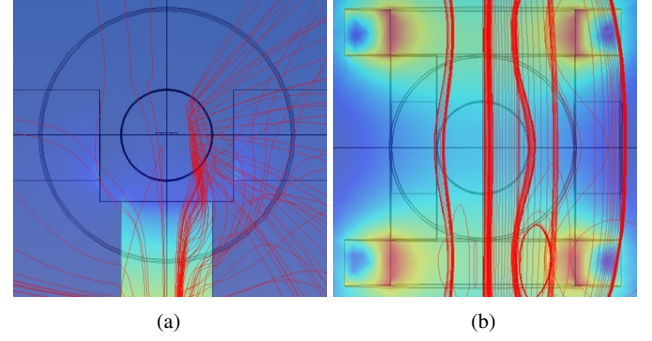

FIGURE 11. Comparison of simulated vertical magnetic field produced by two different types of coil systems. The simulation is run by COMSOL software. (a) The vertical magnetic field of the current coil system design; (b) The vertical magnetic of Helmholtz coil set-up.

agent is able to conquer the 3D features of the dimensions less than the size of microrobot body.

7 Discussion

During the initial proof of concept tests, aspects open to improvements have been identified. For the current electromagnetic coil system, it is impossible for the μTUM agent to tumble over the obstacle of the size comparable to the robot body. However, the tumbling motion is adaptable for the environment in all dimensions. In order to conquer the large size that is comparable to the microrobot or even larger, a top coil can be incorporated into the coil system enclosing the workspace. When the agent encounters a "high wall", the side coil can be on to set the agent to transient state and the top coil used to achieve the tumbling task. A more adaptable μTUM system is expected with an upgraded coil system in our future work.

Further than adding a top coil to enhance the mobility of μTUM, the form of the coil and system structure can also be adjusted. Based on the tests, sliding phenomenon is observed even on the surface with a high friction coefficient, which indicates that the agent experiences considerable lateral magnetic forces when only the bottom coil is turned on. This means the vertical field at the workspace in the current coil system is not perfectly upright. This judgement is also corroborated by the simulation in COMSOL (Fig.11(a)). In the future, Helmholtz coils will be adopted in this tumbling system design. This type of coil system has been applied in some magnetic actuation work at small scales [23–25]. Although the Helmholtz set-up is not compact and the magnetic field it generates is not as strong as the current system for the same current input, the attractive advantage of Helmholtz coil is that it is able to provide magnetic field in a uniform direction in an enclosed workspace (Fig.11(b)).

Another aspect able to be improved lies in the fabrication process. During the polarization tests, not all the robots per-

form as desired, meaning that not all of the fabricated agents have the ideal desired magnetic properties. Because the NdFeB magnetic powder has uniform and reliable magnetic properties, the problem happens during the polarization step during the fabrication. In the polarization step, the permanent magnetic disk was set right underneath the wafer substrate, thus the polarization field can be treated as the field on the surface of magnetic disk. But the field measurement results of the disk show that the field intensity on the surface is not uniform along the radial direction, which means the NdFeB particles in SU8 would experience some lateral forces rather than just pure vertical force along the thickness direction of the sample and disk. Hence, the agents on the substrate position corresponding to large field gradient of the magnetic disk would fail to be polarized as in the proposed design. This drawback can be solved by an improved polarizing magnetic disk. The surface field gradient is dramatic at the fringe part of magnetic disk, so a larger disk will be able to provide more uniform fields in the central region of the wafer.

8 Conclusions

A novel magnetic microrobot system design applying a tumbling mechanism is developed in this work. The μTUM agent of 400 μm total length has a dumbbell structure with two opposite polarized magnetic bell parts. This microrobot is able to perform the tumbling motion driven by a predefined sequence of external magnetic fields which are produced by a coil set consisting of five electromagnetic coils. The key aspects of this mechanism is discussed through the manually controlled experimental results where the translation speed of 0.38mm/s is achieved. Faster speeds can be expected based on an upgraded control system and signal. The most appealing advantage of this μTUM system design is the adaptability to complex environments. The first batch of fabricated prototype agents have shown mobility on various types of surfaces, including 3D structures such as fibrous tissues. This tumbling design at the micro-scale has the potential to be effective tool in real biological and medical applications.

REFERENCES

[1] Gorman, J. J., McGray, C. D., and Allen, R. A., 2009. "Mobile microrobot characterization through performance-based competitions". *Performance Metrics for Intelligent Systems (PerMIS) Workshop*.

[2] Taylor, R. H., 2009. "A perspective on medical robotics". *Proc. IEEE*, **94**(9), Sept., pp. 1652–64.

[3] Donald, B. R., Levey, C. G., McGray, C. D., Rus, D., and Sinclair, M., 2003. "Power delivery and locomotion of untethered microactuatuors". *Journal of Microelectromechanical Systems*, **12**(6), Dec., pp. 947–959.

[4] Donald, B. R., Levey, C. G., McGray, C. D., Paprotny, I., and Rus, D., 2006. "An untethered, electrostatic, globally controllable mems micro-robot". *Journal of Microelectromechanical Systems*, **15**(1), Feb., pp. 1–15.

[5] Donald, B. R., Levey, C. G., and Paprotny, I., 2008. "Planar microassembly by parallel actuation of mems microrbots". *Journal of Microelectromechanical Systems*, **17**(4), Aug., pp. 789–808.

[6] Sul, O. J., Falvo, M. R., Taylor, R. M., Washburn, S., and Superfine, R., 2006. "Thermally actuated untethered impact-driven locomotive microdevices". *Applied Physics Letters*, **89**, p. 203512.

[7] Vollmers, K., Frutiger, D. R., Kratochvil, B. E., and Nelson, B. J., 2008. "Wireless resonant magnetic microactuator for untethered mobile microrobots". *Applied Physics Letters*, **92**, p. 144103.

[8] Frutiger, D. R., Vollmers, K., Kratochvil, B. E., and Nelson, B. J., 2009. "Small, fast, and under control:wireless resonant magnetic micro-agents". *The International Journal of Robotics Research*, **29**, pp. 613–636.

[9] Pawashe, C., Floyd, S., and Sitti, M., 2009. "Modeling and experimental characterization of an untethered magnetic micro-robot". *The International Journal of Robotics Research*, **28**, pp. 1077–94.

[10] Floyd, S., Pawashe, C., and Sitti, M., 2009. "Two-dimensinal contact and noncontact micromanipulation in liquid using an untethered mobile magnetic microrobot". *IEEE Transactions on Robotics*, **25**(6), Dec., pp. 1332–42.

[11] Sliker, L. J., Wang, X., Schoen, J. A., and Rentschler, M. E., 2010. "Micropatterned treads for in vivo robotic mobility". *Journal of Medical Devices, Transactions of the ASME*, **4**, Dec., p. 041006.

[12] Terry, B. S., Lyle, A. B., Schoen, J. A., and Rentschler, M. E., 2011. "Preliminary mechanical characterization of the small bowel for in vivo robotic mobility". *Journal of Biomechanical Engineering, Transactions of the ASME*, **133**, Sept., p. 091010.

[13] Hou, M. T., Shen, H. M., Jiang, G. L., Lu, C. N., Hsu, I., and Yeh, J. A., 2010. "A rolling locomotion method for untethered magnetic microrobots". *Applied Physics Letters*, **96**, p. 024102.

[14] Jiang, G. L., Guu, Y. H., Lu, C. N., et al., 2010. "Development of rolling magnetic microrobots". *Journal of Micromechanics and Microengineering, 20*, p. 085042.

[15] Hemes, B., Canelon, D., Dancs, J., and Papanikolopoulos, N., 2011. "Robotic tumbling locomotion". In International Conference on Robotics and Automation, IEEE, pp. 5063–69.

[16] Griffiths, D. J., 1998. *Introduction to Electrodynamics (3rd ed.)*. Prentice Hall.

[17] Yesin, K. B., Vollmers, K., and Nelson, B. J., 2006. "Modeling and control of untethered biomicrorobots in a fluidic environment using electromagnetic fields". *The International Journal of Robotics Research, 25*, pp. 527–36.

[18] Kummer, M. P., Abbott, J. J., Vollmers, K., and Nelson, B. J., 2007. "Measuring the magnetic and hydrodynamic properties of assembled-mems microrobots". In International Conference on Robotics and Automation, IEEE, pp. 1122–27.

[19] Abbott, J. J., Ergeneman, O., Kummer, M. P., Hurt, A. M., and Nelson, B. J., 2007. "Two-dimensinal contact and noncontact micromanipulation in liquid using an untethered mobile magnetic microrobot". *IEEE Transactions on Robotics, 23*(6), Dec., pp. 1247–52.

[20] Jing, W., Chen, X., Lyttle, S., Fu, Z., Shi, Y., and Cappelleri, D. J., 2010. "Design of a micro-scale magnetrostrictive asymmetric thin film bimorph microrobot". In Internatioanl Mechanical Engineering Congress & Exposition, ASME.

[21] Jing, W., Chen, X., Lyttle, S., Fu, Z., Shi, Y., and Cappelleri, D. J., 2011. "A magnetic thin film microrobot with two operating modes". In International Conference on Robotics and Automation, IEEE, pp. 96–101.

[22] Coey, J. M. D., 2010. *Magnetism and Magnetic Materials*. Cambridge University Press.

[23] Yesin, K. B., Vollmers, K., and Nelson, B. J., 2004. "Analysis and design of wireless magnetically guided microrobots in body fluids". In International Conference on Robotics and Automation, IEEE, pp. 1333–38.

[24] Jeong, S. L., et al., 2010. "Novel electromagnetic actuation (ema) method for 3-dimensional locomotion of intravascular microrobot". *Sensors and Actuators A: Physical, 157*, pp. 118–125.

[25] Jeong, S. L., et al., 2010. "Novel electromagnetic actuation system for three-dimensional locomotion and drilling of intravascular microrobot". *Sensors and Actuators A: Physical, 161*, pp. 297–304.